HOML-SL: IoT Based Early Disease Detection and Prediction for Sugarcane Leaf using Hybrid Optimal Machine Learning Technique

V. Selvakumar
Assistant Professor Department of Computer and Information Science Annamalai University, vselvakumar1921@gmail.com

Dr. Seetharaman
Professor Department of Computer and Information Science Annamalai University

Abstract

Sugarcane is the mostly cultivated crop in Indian agriculture. The quantity and quality of sugarcane production is decreasing day by day due to several diseases. Because of fungi, bacterial, pathogenic, and viral infections often affect crop production with diseases that affect farmers 'economic incomes. In order to increase the quality of the crop, early detection is required. An image processing practice plays a critical role to predict the disease in various plants. In this paper we propose a hybrid optimal machine learning technique (HOML-SL) for detect disease in sugarcane leaf. First, we introduce a non-linear cluster based optimization (NCO) algorithm for segmentation which segments the diseased area from the original sugarcane leaf. Second, we develop an optimal feature selection process using cross layer optimization (CLO) algorithm which select optimal features among multiple features. Finally, we illustrate a moth flame based capsule neural network (MFO-CNN) algorithm to classify the sugarcane leaf disease (such as mosaic virus, red rot, grassy shoot and ring spot). The performance of proposed HOML-SL disease detection can compare with the accessible state-of-art detection techniques in terms of accuracy, precession, F-measure and Recall.

Key words: *early disease detection, cluster based optimization, machine learning, multi feature extraction, classifier.*

1. INTRODUCTION

Sugarcane is a renewable natural agricultural resource as it produces sugar, bio fuels, fiber and fertilizers. Sugar juice is used to make white sugar, brown sugar, jiggery, and ethanol. As a by-product of sugar, this method takes biases and molasses. Molasses can be used as an ingredient in the preparation of alcohol. Additional bias is now used as a raw material in the paper industry. This not only reduces the production of sugar in the skin, but also reduces diversity. To reduce this, crop infections need to be identified and treated in advance. Although there are different types of diseases, the 3 main diseases are rust spots, yellow spots and ring spots. These diseases can be identified by sugarcane leaf spots. The disease can be detected with the naked eye, but using the detection method provides the best evaluation result. The current system uses a digital image of the leaf to diagnose the disease, but not everyone can achieve a high definition digital image. Early and correct analysis of crop sickness is a significant constituent of any crop organization scheme. Plant diseases can be managed more efficiently if control events are taken at an early period of disease growth. The

disease can be diagnosed well before the onset of symptoms, and it is not sufficient to diagnose the symptoms as the symptoms vary considerably. Recent advances in molecular biotechnology are being used to develop rapid, specific, and sensitive tools for the detection and evaluation of plant diseases. The genus Ustilaco of the genus Pseudomycetes contains a group of phytopathogens that cause disease in a variety of plants, including grains. Diabetes mellitus is one of the first to be diagnosed with acidic acid-like fungal infections of infected plants. It arises from the chorionic terminal or from the shoots of the affected stem, which contains the central nucleus of the parenchyma and the vascular host tissue that forms the thin cylindrical telescopes. The life cycle of smart fungus is the same for all organisms and involves changes between three types of cells. Diploid teleospheres are resting cell types, mainly propagated by wind or rain. They occur with the formation of proboscis, of which four disorders occur after mystic. Haploid refers to a rare second cell type. Sugarcane, a hybrid known as sugarcane yellow leaf syndrome (SCYLS), yellow and liver disease is common in many countries. The main symptom of the disease is a yellowish white spot in the middle spreading from the middle to the laminate in reeds aged 6 months and above. In severe cases, diseased plants can be interrupted and easily removed. In some cases, this situation may lead to significant financial losses due to significant crop failure or yield decline. Sugarcane yellow phytoplasma (SCYP), temporarily named phytoplasma, and two factor agents described as sugarcane yellow leaf virus (SCYV) are described in detail in reeds infected with yellow leaf syndrome (YLS).

SCYV is widespread in the United States and neighboring country, making it a major player in SCYL. It is measured a poliovirus of the Ludoviridae people. The virus particle is confined to the sclera hankie and is found in the cytoplasm of rod cells with YLS. Studies on viruses from other crops identified by Bloom indicate that sucrose is impaired in transport, inhibits plant growth and shows no symptoms. Sachs performed diagnostic procedures to detect the Saccharin yellow leaf virus (SCYLV) have been perform using both enzyme linked immunosorbent assay (ELISA) and tissue blot immune-assay (TBIA). Phytoplasma is a flower-specific pathogen that causes negative plant diseases in many crops of different economic meaning to sugarcane. In South Africa, SCYLS is mainly connected with phytoplasma (SCYP), as shown by the polymerase chain reaction (PCR). A small percentage of reeds were infected, and most of them were SCYP infected. Variations in phytoplasma concentrations were observed at different stages of budding and in different samples of sugarcane grassy shoot disease (GSD) tissue. Assessing the severity of plant diseases is an important step in the reproductive process of reeds. In a sugar factory this disease not only reduces the yield but also increases the variety. The amount of sugarcane produced depends on the severity of its disease. About 15% of leaf reeds are diseased and there is a significant loss in reed production. In order to control this disease and reduce the infection in the entire area of the cane, this disease should be detected and treated in advance. The three main types of spot disease affecting tropical crop are rust spot, yellow spot and ring spot. Symptoms of diseases caused by these fungi are obvious spots on the leaves. These sites can be automatically identified based on the characteristics of the spots. However, there are limitations to accepting this guideline, which is often detrimental to the effort. The naked eye cannot self-diagnose and evaluate subjectively and accurately diagnose the disease. The

Internet of Things (IoT) is the connectivity of physical devices, vehicles, home appliances, and other items embedded with electronics, software, sensors, actuators, and network which allow these things to attach and interchange data, generating opportunities for more direct merging of the physical world into computer-based systems, resulting in reduced human intervention. By the year 2050 the global population is set to reach 9.6 billion. So, to nourish this much population, the farming industry must adopt IoT technology. The demand for more food has to be met against the challenges such as intense weather conditions and exhaustive farming practices. Smart farming based on IoT technologies enhances crop production in farming industry.

Our contributions A hybrid optimal machine learning technique (HOML-SL) is proposed to detect the disease in sugarcane leaf. The main objective of proposed HOML-SL disease detection technique is to predict the disease in earlier and the warning information communicate to corresponding farmers on time through IoT. The rest of the paper is organized as follows: Sect 2 describes the recent works related to our contributions. Sect. 3 developed problem methodology and system architecture of proposed disease detection technique. Sect. 4 illustrated the detailed working function of proposed disease detection technique with proper mathematical model. Sect. 5 discussed the simulation results and comparative analysis of proposed and existing classifiers over different performance metrics. Finally, the paper concludes in Sect. 6.

2. Related works

Zhang et al. [21] have proposed an investigated 78 copies of sugarcane collected from four provinces of southern China was collected from four provinces of southern China: Guangxi, Yunnan, Hainan, Guangdong, and 85 percent of the sugarcane plantations in China. We identified 72 hybrid cane specimens with reed mosaic disease components using RT-PCR, sequencing and phylogenetic analysis. Mollov et al. [22] have proposed a Ramu stunt disease of sugarcane was first reported in Papua New Guinea in the mid 1980s. The disease significantly reduces the yield of sugarcane and causes severe stagnation and death in very weak crops. Ramu inquired about the trick agent but his behavior was not enforced. Cane CV Rocker from Pamua New Guinea analyzed the next generation sequence with symptoms of ramostrick. Total RNA was obtained and the entire transcriptase gun sequence was executed using the Illumine site. More than twenty-seven million questions were received, with an average of 100 nucleotides. Avellaneda et al. [23] have proposed a differential genetic study was performed using a repressive minus hybrid to identify genes that can respond to brown oxidation in sugar skin. L99-233 analyzes a sample of the expression of Library 217, which represents biological pathways, genes related to protection, and signal genes, and demonstrates quantitative resistance to the L01-299 resistant genes B1 and Ho 95-988. L09 -125, 24 hours, 48 hours, 72 hours, 1 week b. Post-vaccination dose of P. melanocephala (half) with RT-PCR. All genes have been shown to accumulate news of infection in weak and resistant crops, but maintaining high levels of the gene MRNA for a long time seems to be the most important component of brown rust resistance. Differences were found during gene expression between L01-299 and L99-233. Hamonts et al. [24] have proposed that YCS can play a significant role in the regeneration and meaning of the rhizosphere micro biome. These fluctuations compromise YCS plant protection and alter the root system. In addition, we found a significant decrease in the microbial activity

concerned in DNA / RNA / protein dispensation, but not in the detailed activity concerned in nutrient uptake. In addition, we found a consistent concentration in the encryption of functional genes to protect against pathogens and to alter the root excitants in the rhizosphere of YCS-infected plants, which may reflect an immune rejoinder or a suppressed plant rejoinder. In addition, this study helps to fill the basic awareness gap in the stable rejoinder of microbial handy matching genes of dissimilar stress crops.

Li et al. [25] have proposed the two main causes of mosaic disease are dual confrontation to SCSMV and SRMV once a year in 71 new elite read species / clones in 2015 and 2016. RT-PCR discovery was used to confirm the dearth of the virus. These results are an elite resource for preventing and controlling mosaic disease, and they can be used exclusively for business types. Currently, three viruses, SCMV, SRMV and SCSMV, cause mosaic disease in the Chinese cane region. Symptoms caused by the three viruses are difficult to detect. Ukoskit et al. [26] have proposed a quantitative trait loci (QTL), which validates an association map, was used to determine the EC-Sequence (EST-SSR) identified by the association related to sugar-related properties. For link representation, 524 EST-SSR, 241 amplifier band length polymorphism, and 10 gene SSR markers were combined using 283 F1 lines obtained from the interval. Six locations were identified using multiple QDL maps, but 14 unrelated markers were identified using a single marker analyzer. The association studied 200 approaches based on the mixed linear model. Studies of the EST-SSR markers in the QDL genome group targeted using an association scheme show the correlation between two EST-SSR markers, uridine diphosphate (UDP) glycosyl transferees, beta amylase and sugar. These functional markers can be used with the help of a cane marker. Sheng et al. [27] have proposed the SCMV strain FZ1 vaccine, dual antibody sandwich enzyme-linked immunosorbent, electron transduction electron microscopy, and Bd21 and nicotine in the prototype are systematically inhibited. BD21 leaves developed mosaic symptoms, while N. benthamiana leaves showed no obvious symptoms due to the SCMV-FZ1challenge.

Srivastava et al. [28] have proposed the Inception V3, VGG-16 and VGG-19 have three screens based on the removal of various features. These are ancillary models trained in different taxonomy. Modern algorithms compared to in-depth learning algorithms such as neural network and hybrid cardboard. Orange program calculates a number of statistics such as accuracy, precision, feature, AUC, and sensitivity and selects for high accuracy readings. The characteristic curve of the receiver operation is calculated to determine the accuracy. 90.2% accept AUC as VGG-16 as a character extractor and SVM classifier. Izaías et al. [29] have proposed a during the 2018 harvest cycle, 101 reed samples with YLS symptoms were collected. SCYLV and the new phytoplasma were detected by RT-PCR and local PCR, respectively.

Table 1 Summary of Research gap

Ref.	Species	Methodology	Classifier	Performance improvement
21	Reed mosaic disease	RT-PCR, sequencing and phylogenetic analysis	SrMV, SCMV, and SCSMV	Accuracy

22	Ramu stunt disease	BLAST Algorithm	Six RNAs and RT-PCR amplicons	Accuracy and precession
23	Sugarcane brown rust	Suppressive Subtraction Hybridization	Sequencing and bioinformatics analysis	Accuracy
24	Yellow Canopy Syndrome	DNA extraction and next-generation sequencing, quantitative PCR	Amplicon sequence data, of rhizosphere soil metagenomics data	Accuracy and recall
25	Sugarcane streak mosaic virus (SCSMV) and Sorghum mosaic virus	RT-PCR detection	PCR amplification, cDNA synthesis, Total RNA extraction	Accuracy and recall
26	Expressed Sequence Tag-Simple Sequence Repeats (EST-SSRs)	Linkage and association mapping	241 Amplified Fragment Length Polymorphisms, and 10 genomic SSR markers	Accuracy and precession
27	Sugarcane Mosaic virus	RT-PCR analysis	DAS-ELISA, Back-inoculation	Accuracy and precession
28	Sugarcane plant disease (Mosaic disease, Ring Spot, Grassy Shoot)	BLAST Algorithm	Inception v3, VGG-16 and VGG-19.	Accuracy and F-measure
29	Sugarcane Yellow Leaf Virus	RT-PCR and nested PCR	Sequencing, phylogenetic and recombination analysis	Accuracy and precession
30	Presence of FUM1	Fungal genomic DNA extraction	Validation of Fusarium species	Accuracy and precession

The identification of viral and phytoplasmic positive samples was confirmed by the optimal sequence, which was used in subsequent biogenetic studies. All samples contained two pathogens. The phytoplasma of the nucleotide range of the 16 SRDNA genes shared 99.0% identification with 16 SRVI phytoplasma sequences from Argentina and Brazil. Torres et al. [30] have planned that most Fusarium spp. isolates that are capable of producing fumonisin are from the Visayas Island, another isolated from Luzon. It is noteworthy that the priest is not an SBP. Isolation was found in Mindanao, which provides the FUM1 gene. In previous studies and experiments in which puserium was extracted from muscle grain, many people were able to produce fumonisin. The summary of research gap belongs to related works are tabulated in Table

3. Problem methodology and system architecture

3.1 Problem methodology

Sugarcane is the most traditional and economically important major crop in Louisiana. Parts of the stalk are planted with buds to replace the original seeds. Diseases caused by pathogenic bacteria, fungi and

viruses can adversely affect sugar. Some of our most important diseases are caused by systemic pathogens.

3.1.1 Fungal Disease

- Red rot disease: It is caused by Colletotrichum falcatum and Fig. 1a shows the model leaf. This fungus is more strongly beneficial than a parasite and cannot attack healthy canes, but it will molest the young sugarcanes. Red rot is difficult to control because the seed-producing stalk is often affected by the time of planting and the fungicides fail to reach the affected tissues in the diseased seed colony.

- Sugarcane smut disease: It is cause by fungus, Ustilago scitaminea, shows in Fig. 1b. Sugarcane smut is easily recognizable by its black whip-like structure that develops from the site of growth of the sugarcane plant. It is spread mainly by airborne spores or infected or contaminated cane cuttings.

- Sugarcane wilt disease: The symptoms of this disease are similar to those of red rot disease, which often interferes with two diseases of farmers and shows in Fig. 1c. The wilt disease cycle is Perennation and Infection. The sugarcane wilt disease is caused by Fusarium sacchari.

- Pineapple disease: It is caused by Ceratocystis paradoxa, shows in Fig. 1d. The affected tissue is reddened in the first place; the parenchyma then disintegrates and becomes hollow and black inside the set. An infected set of pineapples may disintegrate until the buds stop or die again when young shoots appear.

- Common rust: It is caused by Puccinia melanocephala, shows in Fig. 1e. The symptom of common rust on the cane is long yellow leaf spots, 1-4 mm. In prone plants the spots increase in size and turn reddish brown.

- Orange rust: It is caused by Puccinia kuehnii, shows in Fig. 1f. Common symptoms range from cinnamon to a yellowish-brown sore with persistent burns and sometimes spots on the underside of leaves. It does not concern red raspberries.

- Top rot: It is caused by Fusarium proliferatum, shows in Fig. 1g. Leaf strips and top rot can occur separately or together in a field with relatively high atmospheric humidity.

Fig. 1. Sugar leaf fungal disease (a) red rots disease (b) smut disease (c) wilt disease (d) pineapple disease: (e) common rust (f) orange rust and (g) top rot

(a) (b) (c) (d) (e) (f) (g)

3.1.2 Bacterial diseases

- Ratoon stunting disease: It is cause by Leifsonia (Clavibacter) Xyli, shows in Fig. 2a. In this, the infected stems are usually stunted and yellowish-green.

- Leaf scald: It is caused by Xanthomonas albilinean, shows in Fig. 2b. The symptoms include two major forms, chronic and acute, with two distinct stages: delay and eclipse.

- Grassy shoot disease: It is caused by Candidatus phytoplasma, shows in Fig. 2c. Symptoms of the disease appear immediately on the resulting shoots.

Fig. 2. Sugar leaf Bacterial disease (a) ratoon stunting disease (b) leaf scald and (c) grassy shoot disease

(a) (b) (c)

3.1.3 Viral diseases

- Yellow leaf disease: It is cause by the sugarcane yellow leaf virus, shows in Fig. 3a. YLD-infected sugar plants reduce photosynthetic activity; reduce photosynthesis from leaves to zinc, thereby reducing the accumulation of sucrose in the affected stem.

- Sugarcane mosaic: It is cause by Sugarcane streak mosaic virus, shows in Fig. 3b. Then, 6 weeks after transplanting, the weak and moderately hardy sugar leaves were automatically inoculated with SCMV.

- Leaf fleck: It is caused by the bacilliform virus, shows in Fig. 3c. A fleck is most important at the edge of the leaf and the distal end of the leaf. Suspicious pattern, modelling, and symptoms of light mosaic associated with viral infection. . This disease is spread through the infected seeds and mealy bug.

Fig. 3. Sugar leaf Viral disease (a) yellow leaf (b) sugarcane mosaic and (c) leaf fleck

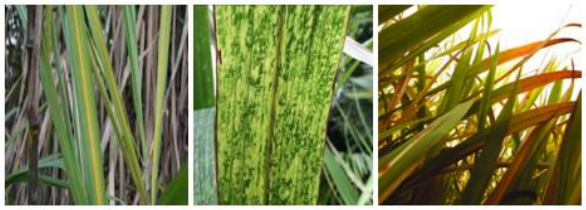

(a) (b) (c)

3.2 System architecture of HOML-SL technique

Fig. 4 describes the complete model for disease detection on sugarcane based on image processing. The input image is taken from the sugarcane leaf. At first the preprocessing technique is used to suppress some images for additional process. The Nonlinear cluster based optimization is used to segment the disease affected part from unhealthy leaf. The feature extraction is used to describe the edge, corner, shape and color of the leaves. The most relatable part is determined by optimal feature selection using cross layer optimization. Finally the disease is classified using Moth flame optimization-capsule neural network in terms of red spot, mosaic virus, ring spot, grassy shoot and healthy leaf.

4. Hybrid optimal machine learning technique for sugarcane leaf disease detection (HOML-SL)

4.1 Segmentation using non linear clustering based optimization algorithm

Segmentation is the process of separating the data from a group. In leaf disease, segmentation technique separates the diseased part from the healthy leaf with the best accuracy ratio. Segmentation is an important step in image processing techniques for identifying the affected area. Clustering is said to be grouping of leaves that is diagnosed with disease. By using this clustering methodology, we able to predict the disease at initial stage. By identifying the disease earlier, we can segment both healthy and disease affected areas in leaf. Consider that feature vectors are N real space in size and k feature vectors are in space.

Fig. 4. System model of proposed disease detection technique

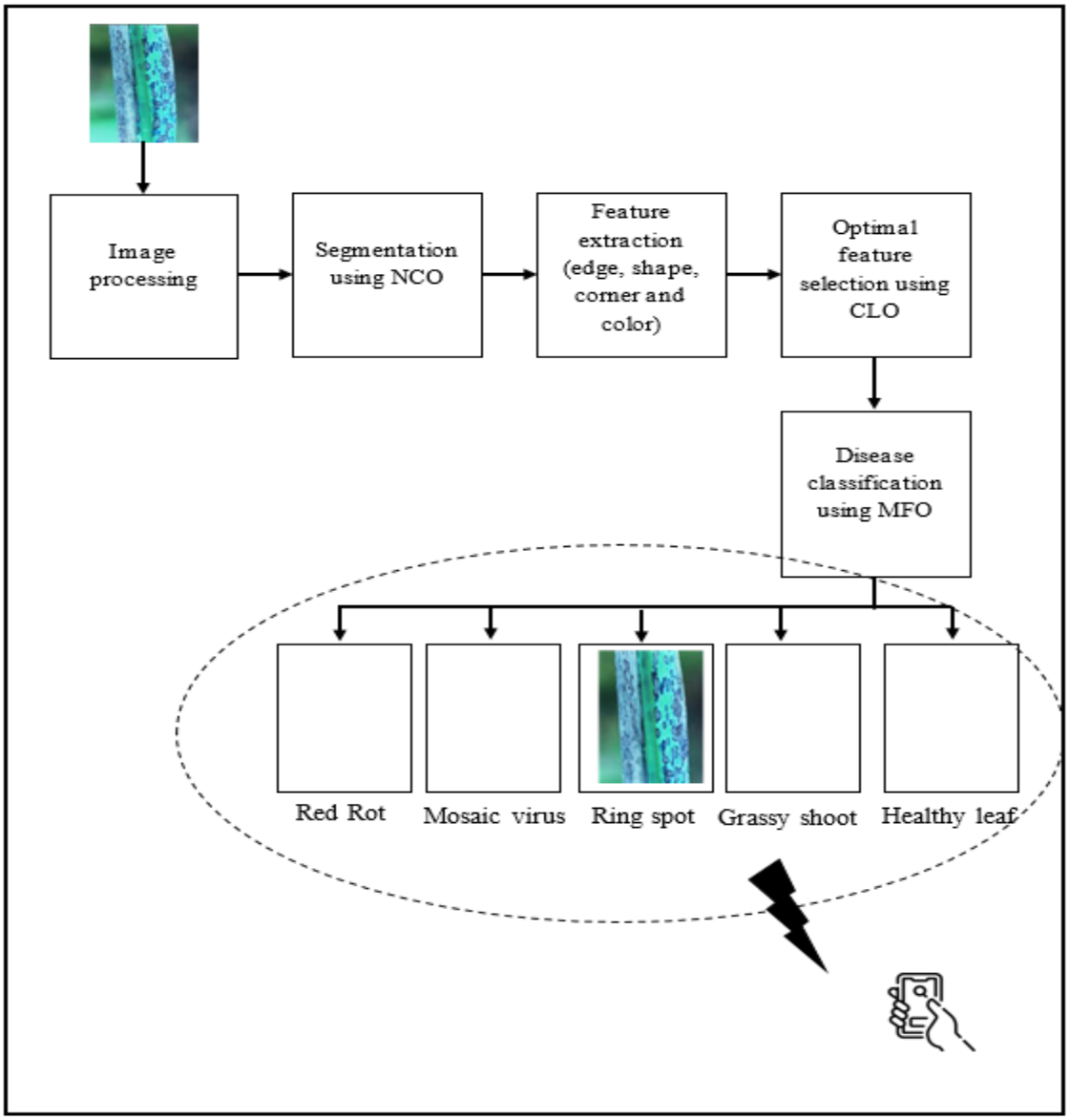

Imagine these feature vectors be y_l for l=1, 2, …, L. If there are N clusters. Assume that the vectors denoting these clusters at the q^{th} iteration of the algorithm be $\mu_{q,n}$ for n=1, 2,.., N and for $q \geq 0$. Then define,

$$Y = [y_1, ...y_l] \qquad for\ q \geq 0 \tag{1}$$

$$\mu_q = [\mu_{q,1}, ...\mu_{q,N}] \quad for\ q \geq 0 \tag{2}$$

Let the coefficient indicating the project of y_l to $\mu_{q,n}$ at the q^{th} iteration of the algorithm be $d_{q,l,n}$ for l=1,….L, for n=1,…..,N and for $q \geq 0$. If Y_l is allotted to $\mu_{q,n}$ at the q^{th} iteration of the algorithm, then $d_{q,l,n} = 1$ for l=1,…..,L , for n=1,…..,N and for $q \geq 0$. Or else, $d_{q,l,n} = 0$ for l=1,…..,L , for n=1,…..,N and for $q \geq 0$. Therefore, $d_{q,l,n} \in \{0,1\}$ for l=1,…..,L , for n=1,…..,N and for $q \geq 0$. Let $d_{q,l} = [d_{q,l,1}, ..., d_{q,l,N}]^t$ for l=1,.,L , for n=1,…..,N and for $q \geq 0$. It should be noted that only one non-zero element is equal to one in $d_{q,l}$ for l=1,…,L and for $q \geq 0$. This non-zero component represents the y_l cluster code. Likewise, imagine $d_q = [d_{q,1}, ..., d_{q,L}]$ for $q \geq 0$ For the k_2 clustering optimization algorithm, define

$$\| W \|_2^2 = \sum_{l=1}^{L} \| W_l \|_2^2 \qquad where\ W = [w_1, ..., w_L] \tag{3}$$

As q=0, the index of iteration is initialized and the algorithm as $\in > 0$ is terminating as constant, and for the 0^{th} iteration of the algorithm, the clusters are indicated using the matrix as, $\mu_0^* = [\mu_{0,1}^*, ..., \mu_{0,N}^*]$. The q^{th} iteration of the algorithm is formulated with the mission of y_l to $\mu_{q,n}^*$ by the following quadratic integer programming problem,

$$\underset{d_q}{MIN}\, I_{\mu_q^*}(d_q) = \| Y - \mu_q^* d_q \|_2^2 \tag{4}$$

subjected to $d_{q,l,n} \in \{0,1\}$ for l=1,…..,L , for n=1,…..,N and for $q \geq 0$, and $\sum^{N} d_{q,l,n} = 1$ for l=1,…..,L and for $q \geq 0$.Using the equation (5), the initial value is taken and obtain each denoting vector $d_{q,l}(1 \leq l \leq L)$, then the d_q is created by $d_{q,l}$.

$$d_0 = (\mu_0^{*t} \mu_0^*)^{-1} \mu_0^{*t} Y \tag{5}$$

The design of the vectors representing the clusters is designed as the next two-step programming complex. The μ_q is updated in the equation (6),

$$\underset{\mu_q}{MIN}\, I_{d_q^*}(\mu_q) = \| Y - \mu_q d_q^* \|_2^2 \tag{6}$$

Then, the algorithm is terminated when,

$$I_{\mu_q^*}(d_q^*) - I_{\mu_{q+1}^*}(d_q^*) \leq \in \tag{7}$$

Or else, the value of q is incremented. Then, the analysis of convergence is required and the algorithm is iterative. The $I_{\mu_{q+1}^*}(d_q^*)$ and $I_{\mu_q^*}(d_q^*)$ are less bounded, then the condition of the equation () is changed as follows,

$$I_{\mu_q^*}(d_q^*) \geq I_{d_q^*}(\mu_{q+1}^*) \geq I_{\mu_{q+1}^*}(d_{q+1}^*) \geq I_{d_{q+1}^*}(\mu_{q+2}^*) \quad (8)$$

Here, $I_{\mu_q^*}(d_q)$ and $I_{d_q^*}(\mu_q)$ are lower monotonic.

Algorithm 1 Non-linear clustering based on optimization algorithm

Input : μ_q, d_q, y_l

Output : $\underset{\mu_q}{MIN} \; I_{d_q^*}(\mu_q)$

1	Initialize the value for the inputs μ_q, d_q, y_l
2	For l=1,
3	The condition is satisfied i.e. $\sum^{N} d_{q,l,n} = 1$
4	Using the equation (6), compute the value for the one norms
5	End for
6	Compute the value for the two norms.
7	Value for the infinite norm is calculated using the equation (11)
8	End procedure

Now, consider a case where one criterion is used instead of two. The equation contains the two norm criterion.

$$\underset{d_q}{MIN} \; I_{\mu_q^*}(d_q) = \| Y - \mu_q^* d_q \|_1^1 = \sum_{l=1}^{L} \| Y_l - \mu_q^* d_{q,l} \|_1^1 \quad (9)$$

Here, the mixed integer programming method is used. Then, {1,…..L} is partitioned into N subsets denoted as J_n for n=1,….,N. In this, $\forall l_j \in \{1,...,L\}$ for each $n \in \{1,...,N\}$ and if $d_{q,l,n}^* = 1$ then $l_j \in J_n$. Using the linear programming the equation as follows:

$$\underset{\mu_q}{MIN} \; I_{d_q^*}(\mu_q) = \| Y - \mu_q d_q^* \|_1^1 = \sum_{n}^{N} \| y_l - \mu_q d_{q,l}^* \|_1^1 = \sum_{n=1}^{N} \sum_{l \in J_n} \| y_l - \mu_q d_{q,l}^* \|_1^1 \quad (10)$$

Let us now consider the case where the infinite norms criterion is used instead of two norms criteria.

$$\underset{d_q}{MIN} \; I_{\mu_q^*}(d_q) = \| Y - \mu_q^* d_q \|_\infty^\infty = \sum_{l=1}^{L} \| y_l - \mu_q^* d_{q,l} \|_\infty^\infty \quad (11)$$

Here, the integer programming method is used. Then, {1,…..L} is partitioned into N subsets denoted as J_n for n=1,….,N. In this,

$\forall l_j \in \{1,...,L\}$ for each $n \in \{1,...,N\}$ and if $d^*_{q,l,n} = 1$ then $l_j \in J_n$. The termination of the algorithm as follows,

$$\underset{\mu_q}{MIN} \quad I_{d_q^*}(\mu_q) = \| Y - \mu_q d_q^* \|_\infty^\infty = \sum_{n=1}^{N} \| y_l - \mu_q d^*_{q,l} \|_\infty^\infty = \sum_{n=1}^{N} \sum_{l \in J_n} \| y_l - \mu_q d^*_{q,l} \|_\infty^\infty \tag{12}$$

Hence, the algorithm is converged in the infinite norms. Algorithm 1 gives the working function of segmentation based on nonlinear clustering based on optimization algorithm.

4.2 Optimal feature selection using cross layer optimization algorithm

In this segment, we concentrate on feature extraction and optimal feature assortment process. Generally, biometric based authentication for continuous monitoring system gives multiple feature and size, color, thickness, length, and images. This feature provides more than 100 sub features. But, those features are not required for our objective function. So, we need proper feature selection technique to optimize features which reduces computational complexity and better optimal solution. The proposed cross layer optimization based optimal feature selection is proposed to solve those problems. Consider a dynamic system that controls time events (epochs). In each age a decision is made to classify this system as one of the possible states. We understand the state of the system by,

$$T_y = \left\{ \vec{y} \in J_+^N : \vec{y} \in T \right\} \tag{13}$$

At decision epoch s, when a new user comes to the computer with users in that state $y(s)$, two actions must be selected for the new user, i.e. accept or reject. Then the exploit space B_y of a given state $\vec{y}$

$$B_y = \left\{ \vec{b}(b_1,...b_N) : b_n = 0 \ \ if \ \ y + d_n \notin S_y \right\} \tag{14}$$

where $b_n \in \{0, 1\}$, $n \in 1,2,..., N \cdot d_n$ is a vector of zeros apart from for an one in the n-th article. Note that $\vec{b} \neq (0,0,...,0)$ when $\vec{x} = (0,0,...,0)$, or else new associations are never admit into the network and the structure cannot develop. The probabilities $Q(x|y,b)$ of the entrenched chain and the predictable sojourn time $\tau_{y,b}$ for each state-action pair. The state conversion probabilities is defined as

$$Q(x|y,b) = \begin{cases} \lambda_n b_n \tau_{ya}, \vec{x} = \vec{y} + d_n \\ y_n \mu_n \tau_{ya}, \vec{x} = \vec{y} - d_n \\ 0, \quad otherwise \end{cases} \tag{15}$$

where λ_n and μ_n are the typical arrival rate and evaporation rate of class-m users correspondingly, and

$$\tau_{ya} = \left[\sum_{n=1}^{N} y_n \mu_n + \lambda_n b_n \right]^{-1} \tag{16}$$

The maximum throughput is obtain by solving the following linear indoctrination

$$MAX \sum_{y \in T_y} \sum_{b \in B_y} \sum_{n \in N} \varpi_n y_n \tau_{yb} f_{yb} \tag{17}$$

where ϖ_n is the weight of class-m traffic. γ_n is the utmost allowable class-m jamming probability. f_{yb} is the long-run fraction of

result epochs at which the system is in state y and exploit b is made. The first two sets of restrictions refer to the state balance. At the same time, the third set of inequalities is related to CAC-layered barriers. Note that we can return the objective purpose in with $\sum_{n=1}^{N}\varpi_n(1-b_n)$ .This leads to a minimization problem which is given by

$$Min \sum_{y\in T_y}\sum_{b\in B_y}\sum_{n\in N}\varpi_n(1-b_n)\tau_{yb}f_{yb} \quad (18)$$

We use Physical-layer constraints to determine the state position of access policies. Otherwise the cross-layer optimization can be formulate by count,

$$\sum_{y\in T_y}\sum_{b\in B_y}\Pr(SINR_n<\zeta_n)\tau_{yb}f_{yb}\le\varepsilon_n \quad (19)$$

to the constraint of linear programming and important a new state space as

$$F_y=\left\{\vec{y}\in J_+^n: y_n\le K\right\} \quad (20)$$

where n =1,2,..., N and K is an agreed big integer. This work yields similar results to linear programming; however, processing time will be longer as the size of the new state space increases. In this system each user can exceed the N rate. Accordingly, the state has provided space is given by

$$T_y=\left\{(y_t,\vec{y}):\vec{y}\in J_+^N,\vec{y}\in T\right\} \quad (21)$$

where $y_t=\sum_{n=1}^{N}y_n$ is the total number of user in the system. Then, the stroke space of state y is

$$B_y=\left\{b\in[0,1]:b=0\ if\ [y_t+1,\vec{y}+d_n]\notin T_y\right\} \quad (22)$$

where d_n is a vector of zeros excluding for an one in the Nth column (the last column). Let α_n be the evolution rate from state n to $n+1$ and δ_n be the rate from state n to $n-1$. We distinguish the state conversion probabilities by

$$Q(x|y,b)=\begin{cases}\lambda b\tau_{yb}, & \vec{x}=[y_t+1,\vec{y}+d_n]\\ \mu y_n\tau_{yb}, & \vec{x}=[y_t+1,\vec{y}-d_n]\\ \alpha_n(y_t-y_n)\tau_{yb}, & \vec{x}=[y_t,\vec{y}+d_n]\\ \delta_n y_n\tau_{yb}, & \vec{x}=[y_t,\vec{y}-d_n]\\ 0 & otherwise\end{cases} \quad (23)$$

where the predictable sojourn time τ_{yb} is

$$\tau_{yb}=\left[\lambda b+\mu y_t+\sum_{n=1}^{N}\alpha_n(y_t-y_n)+\sum_{n=1}^{N}\beta_n y_n\right]^{-1} \quad (24)$$

The optimization quandary for an N/N system is formulated by the linear programming. The algorithm 2 describes the working function of the Cross layer optimization based on optimization algorithm.

Algorithm 2 Optimal feature selection using cross layer optimization

Input	: x, y, d, μ, λ
Output	: $T_y, B_{y,} \tau_{yb}$
1	Initialize the value for the inputs x, y, d, μ, λ
2	Compute the value of T_y *and* B_y
3	Obtain the throughput in the equation (17)
4	Apply the linear programming in the equation (20)
5	Compute the stock space in the equation (22)
6	Evaluate the predictable sojourn time in the equation (24)
7	End

4.3 Classification using hybrid moth-flame optimization and capsule neural network (MFO-CNN)

Sugarcane is a perennial grass in the family Phocaea grown for its stem (cane) which is chiefly used to create sucrose. The leaves of the plant grow from the tips of the stalks, arranged in two rows on either side of the stalk. Leaves tubular, knife-like, thicker at the margins and around the stalk. The disease detection is needed to enhance the growth of sugarcane crop, which gives continues monitoring the health condition. In this paper, we utilized the hybrid moth-flame optimization and capsule neural network (MFO-CNN) for leaf disease classification. Capsule neural network (CNN) manages transient patterns and has internal memory to process transient sequences automatically. This type of network has feedback that can store information about past behavior. Basically, by collecting neurons, a capsule is formed in which the detection potential is prearranged as a characteristic relative to the length of the output vector. In the CNN, each of its layers contains multiple capsules with different characteristics. CNN stores complete information. In the case of capsule networks, the pillow layers replace the compressed neural networks. Under the "routing by agreement", releases are sent to all close relative capsules and successive layers with dissimilar pairing ratios. If A_j is the output of the capsule j, then the parent capsule i, is evaluate using,

$$\widehat{A}_{i/j} = Z_{ji} A_j \qquad (25)$$

where 'Z_{ji}' is the weight matrix to be cultured through backward pass and $\widehat{A}_{i/j}$ specify the output vector of the i-th capsule.

$$DD_{ji} = \frac{e^{f_{ji}}}{\sum_n e^{f_{jl}}} \qquad (26)$$

where ' f_{ji} ' indicate the log likelihood among capsule j and i and is set to '0' through the start of the routing procedure. Calculates the parent capsule input vector,

$$y_i = \sum_j DD_{ji} \widehat{A}_{i/j} \qquad (27)$$

The non-linear squash function is used to ensure that the capsule release vectors do not go above 1 and that the ending output of each initial capsule is generated based on the initial vector value obtained in Eq. (3)

$$x_i = \frac{\|y_i\|^2}{1+\|y_i\|^2} \frac{y_i}{\|y_i\|} \qquad (28)$$

where' x_i ' indicate the capsule output and ' y_i ' indicate the input vector given to capsule i. consider Esq. (1) and (4), the routing conformity ' RA_{ji} ' to inform the pairing coefficient and log probability is agreed by,

$$RA_{ji} = x_i \bullet \widehat{A}_{i/j} \qquad (29)$$

Capsules 'L' here in the last layer are linked with that of a loss meaning ' kb_l '. This chairs high defeat on the capsules when the article does not exist. The loss utility is compute using,

$$b_l = \theta_l MAX\ (0, n^+ - \|x_l\|)^2 + \lambda(1-\theta_l)\, MAX\ (0, \|x_l\| - n^-)^2 \qquad (30)$$

where ' θ_l ' is '1′ when capsule k is present and is '0′ if it is not present. The parameters λ, n^+ and n^- are the hyper parameter that are to be particular previous to capsule learning. We create a function of the shared value of the network system; it has many error functions related to different pattern points. Therefore, we used the moth-flame optimization algorithm to adjust the network settings to improve error performance. The array of moths represent by a matrix is shown below.

$$N = \begin{bmatrix} n_{1,1} & n_{2,1} & \cdots & \cdots & n_{1,D} \\ n_{2,1} & n_{2,1} & \cdots & \cdots & n_{1,D} \\ \vdots & \vdots & \vdots & \vdots & \vdots \\ n_{n,1} & n_{n,2} & \cdots & \cdots & n_{n,D} \end{bmatrix} \qquad (31)$$

where m is the figure of moths, and D is the dimensions. The intention functions principles achieve by all answer vectors are store in an array.

$$AN = \begin{bmatrix} AN_1 \\ AN_2 \\ \vdots \\ AN_3 \end{bmatrix} \qquad (32)$$

In addition to the properties of the moths, another part of the mechanism is the flame. Assume that the spatial position of the Moon coincides with the wave, and the following matrix is obtained.

$$B = \begin{bmatrix} B_{1,1} & B_{2,1} & \cdots & \cdots & B_{1,D} \\ B_{2,1} & B_{2,1} & \cdots & \cdots & B_{1,D} \\ \vdots & \vdots & \vdots & \vdots & \vdots \\ B_{n,1} & B_{n,2} & \cdots & \cdots & B_{n,D} \end{bmatrix} \qquad (33)$$

Where n is the number of months and d is the measure. Accordingly, we continuously store the functional exercise values of the flame vectors in each group.

$$AB = \begin{bmatrix} AB_1 \\ AB_2 \\ \vdots \\ AB_3 \end{bmatrix} \quad (34)$$

The difference is that the properties fly around the place of search, circling the flame, in which the flame is considered constant and unchanging. In other words, the properties can be reached at their best by the constant movement of the flame. Therefore, only the flame level can be updated for months. Its mathematical model is shown in the next formula,

$$N_j = T(N_j, B_i) \quad (35)$$

where N_j represent the j-th moth, B_j represent the i-th flame and T indicate the spiral functions. The logarithmic spiral is premeditated as follows

$$T(N_j, B_i) = C_j \bullet e^{fS} \bullet COS(2\pi t) + B_i \quad (36)$$

where C_j denotes the coldness between the j-th moth and the i-th flame, s is a random number in [-1, 1], and f is a constant for important the shape of the logarithmic spiral. C_j is definite as follows:

$$C_j = \left| B_i - N_j \right| \quad (37)$$

The logarithmic spiral is a model of the helical flight path of moths around a flame. Based on this formula, we can further determine the position of the Moon in its flight and find that the position of the moths depends on the firing. In the logarithmic spiral function, the position modify of moths is only connected to the location of flame. Therefore, it will increase the chances of falling together to the local optimum. To avoid this problem, an adaptive function was introduced as shown below. The change in the nature of the moon is related only to the position of the flame. Therefore, it will increase the chances of falling together to the local optimum. To avoid this problem, an adaptive function was introduced as shown below.

$$flame\_no = round(M - k * \frac{M-1}{S}) \quad (38)$$

where S indicate the utmost number of iteration, k refers to the recent number of iteration, and M is the utmost figure of conflagration. The algorithm 3 illustrated the working function of the moth flame optimization and capsule neural network based on optimization algorithm.

Algorithm 3 Disease prediction using MFO-CNN classifier

Input : Capsule vector y_i,weight matrices Z_{ji}

Output : Capsule vector x_i, A_j output of the capsule

1. Computational algorithm start
2. $\widehat{A}_{i/j} = Z_{ji} A_j$
3. $f_{ji} \leftarrow 0$

4. While Route Agreement NOT met DO
5. $$DD_{ji} = \frac{e^{f_{ji}}}{\sum_n e^{f_{jl}}}$$
6. End For
7. Initialize the best position of each moths $N_j = T(N_j, B_i)$
8. Adaption of MFO-CNN is represented by

$$T(N_j, B_i) = C_j \bullet e^{fS} \bullet COS(2\pi t) + B_i$$

9. Update the function and position C_j, $C_j = \left| B_i - N_j \right|$
10. Evaluate each of the moths in population and update the best position
11. Update the secondary repository
12. End

5. Result and Discussion

In this segment, we analyze the presentation of planned disease detection technique using set of real time data's which consists of five different classes are healthy, red rot, mosaic, ring spot and grassy shoot diseases. The data collection and image acquisition plays an essential part for proper functioning. From Mawana Sugar Mill Pvt. Ltd, we can gather the images of the diseased and non diseased sugarcane which are used as datasets for this case. The training set contains 160 images and the test sets contain 80 images and these are the classification of sets. The summary of dataset descriptions is given in Table 2. The presentation of planned MFO-CNN classifier is compare with the existing classifiers are neural network (NN), support vector machine (SVM), stochastic gradient descent (SGD), k nearest neighbor (KNN), naive Bayes (NB) and AdaBoost, logistic regression (LR) and classifiers in terms of different metrics are area under curve, accuracy, precession, f-measure and recall.

Table 2 Description of dataset

Details	Category	No. of images
Training set	Diseased	80
	Non diseased	80
Total		160
Test set	Diseased	40
	Non diseased	40
Total		80
Entire dataset		240

Fig. 5. Red rots disease detection

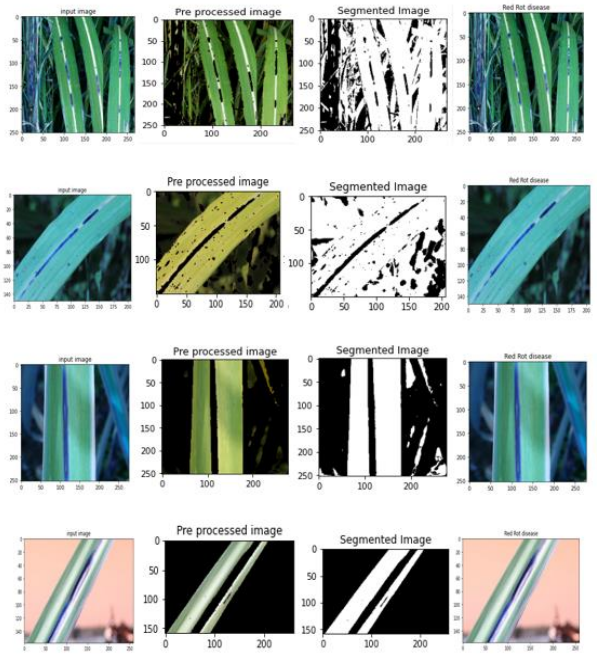

The working function of preprocessing, segmentation and feature extraction are analyzed through following section. Fig. 5 shows the red rot disease detection with preprocessing, segmentation and feature extraction with different set of input picture leaf. Fig. 6 shows the mosaic disease detection with preprocessing, segmentation and feature extraction with different set of input image leaf. Fig. 7 shows the ring spot disease detection with preprocessing, segmentation and feature extraction with different set of input image leaf. Fig. 8 shows the grassy shoot disease detection with preprocessing, segmentation and feature extraction with different set of input image leaf. Fig. 9 shows the healthy detection with preprocessing, segmentation and feature extraction with different set of input image leaf.

Fig. 6. Mosaic disease detection

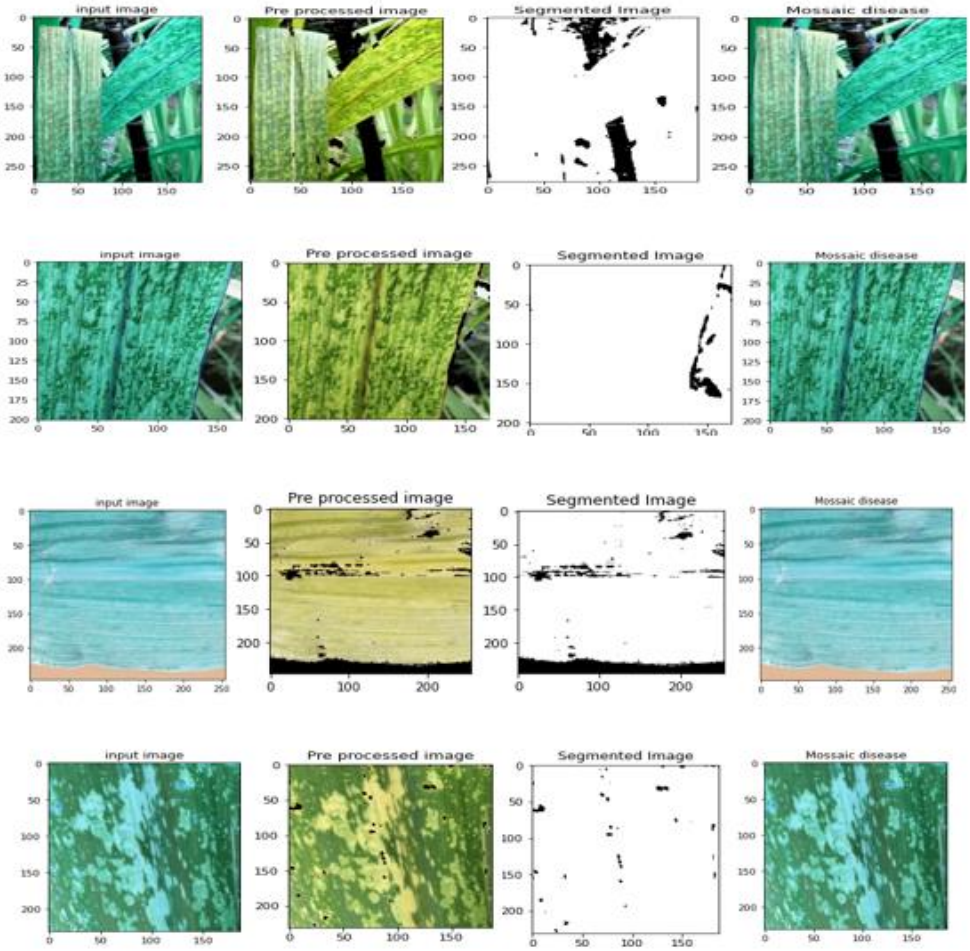

Fig. 7. Ring spot disease detection

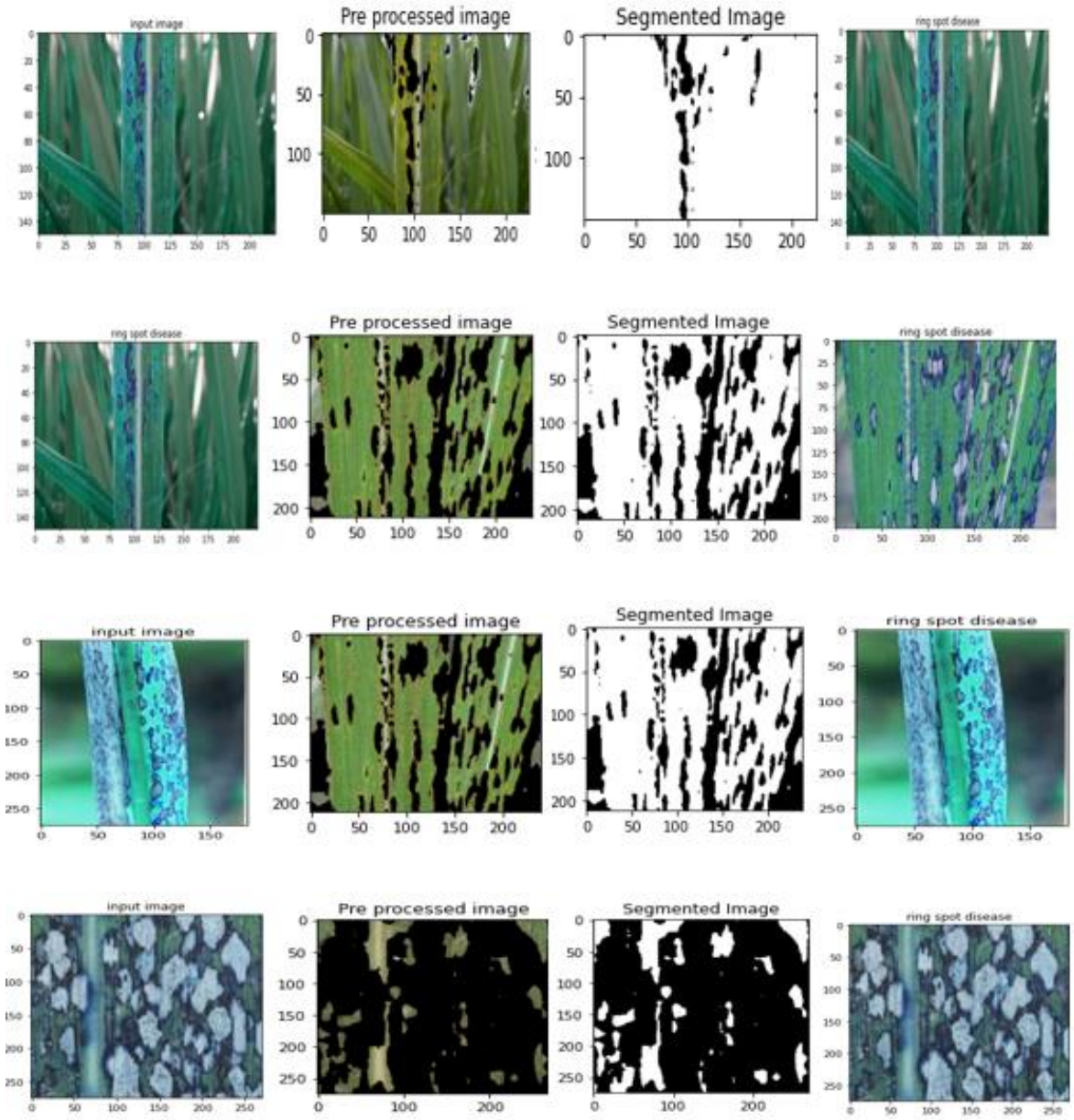

Fig. 8. Grassy shoot disease detection

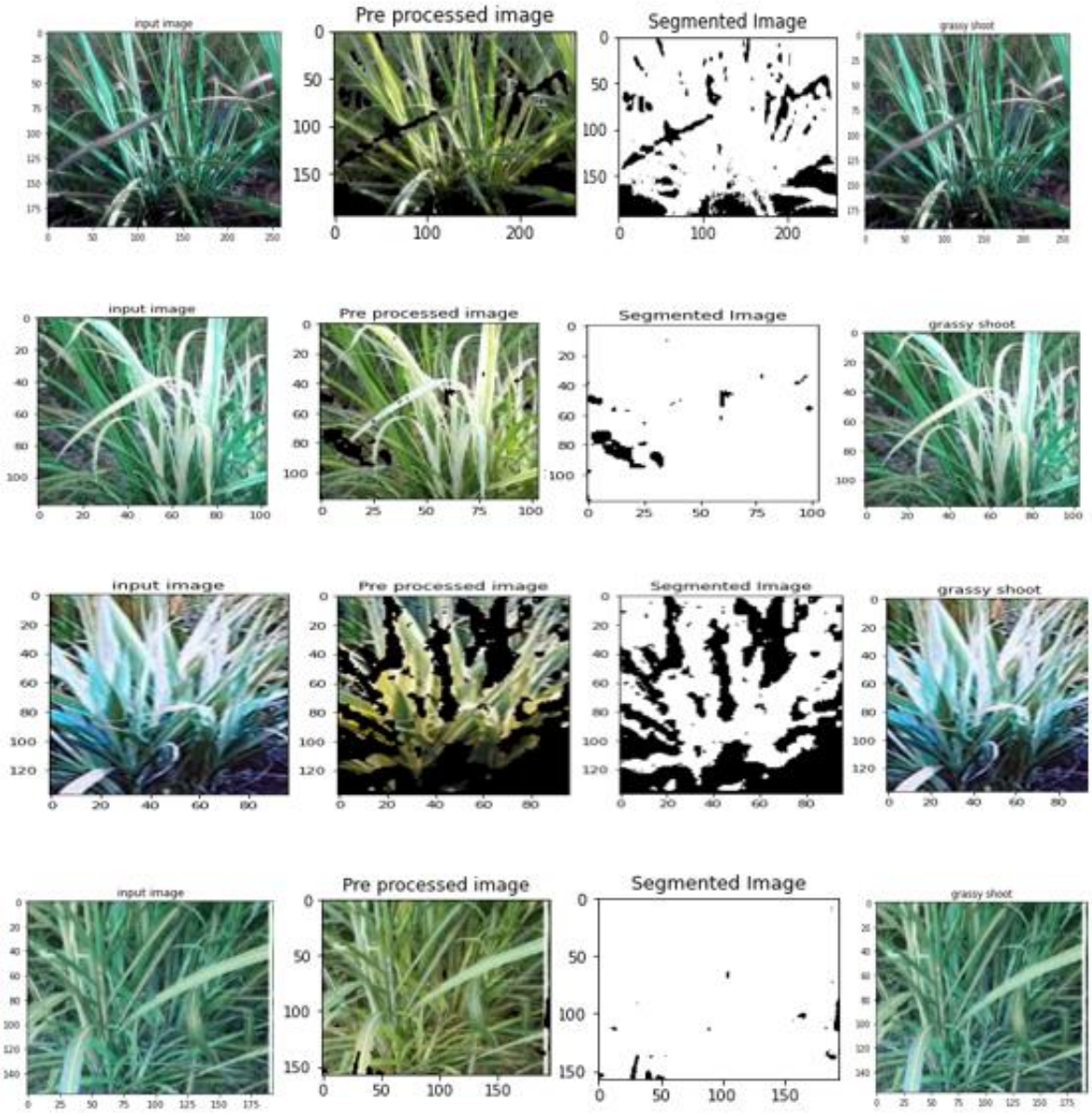

Fig. 9. Health leaf detection

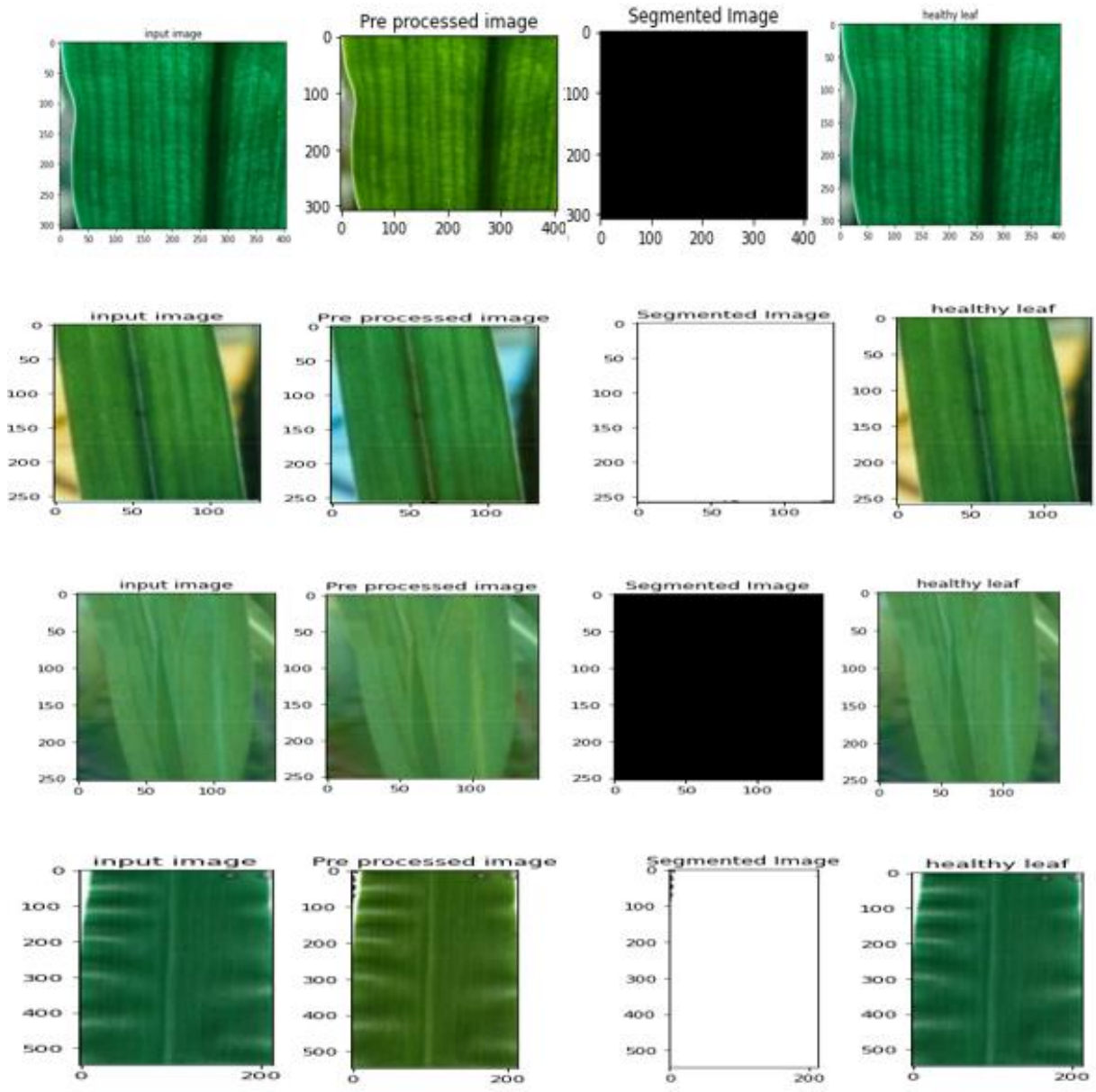

5.1 Comparative analysis

The area under curve of proposed MFO-CNN classifier is 6.7%, 3% and 3% higher than the VCG16 LR, VCG19 LR and inception V3 LR classifier respectively. The area under curve of proposed MFO-CNN classifier is 5%, 5% and 6% higher than the VCG16 SVM, VCG19 SVM and inception V3 SVM classifier respectively. The area under curve of proposed MFO-CNN classifier is 15%, 9% and 14% higher than the VCG16 SGD, VCG19 SGD and inception V3 SGD classifier respectively. The area under curve of proposed MFO-CNN classifier is 4%, 4% and 5% higher than the VCG16 NN, VCG19 NN and inception V3 NN classifier respectively. The area under curve of proposed MFO-CNN classifier is 5%, 4% and 3% higher than the VCG16 KNN, VCG19

KNN and inception V3 KNN classifier respectively. The area under curve of proposed MFO-CNN classifier is 14%, 15% and 15% higher than the VCG16 NB, VCG19 NB and inception V3 NB classifier respectively. The area under curve of proposed MFO-CNN classifier is 5%, 4% and 20% higher than the VCG16 Adaboost, VCG19 Adaboost and inception V3 Adaboost classifier respectively. The Accuracy of proposed MFO-CNN classifier is 12%, 10% and 12% higher than the VCG16 LR, VCG19 LR and inception V3 LR classifier respectively. The Accuracy of proposed MFO-CNN classifier is 11%, 12% and 14% higher than the VCG16 SVM, VCG19 SVM and inception V3 SVM classifier respectively. The Accuracy of proposed MFO-CNN classifier is 15%, 9% and 14% higher than the VCG16 SGD, VCG19 SGD and inception V3 SGD classifier respectively. The Accuracy of proposed MFO-CNN classifier is 12%, 11% and 16% higher than the VCG16 NN, VCG19 NN and inception V3 NN classifier respectively.

Table 3 Comparative analysis of proposed and excising classifiers

Classifiers	Performance metrics (%)				
	Area under curve	Accuracy	F measure	Precession	Recall
Inception v3 LR	91.7	83.8	83.7	83.8	83.8
Inception v3 SVM	89.7	81.9	81.8	82.7	81.9
Inception v3 SGD	81.9	81.9	81.9	81.9	81.9
Inception v3 NN	90.3	80.0	80.0	80.0	80.0
Inception v3 KNN	92.3	79.4	79.3	79.6	79.4
Inception v3 NB	80.2	75.6	75.6	75.8	75.6
Inception v3 Adaboost	76.2	72.5	72.5	72.6	72.5
VGG 19 LR	92.3	85.0	85.0	85.1	85.0
VGG 19 SVM	90.2	83.8	83.7	84.5	83.8
VGG 19 SGD	86.3	86.3	86.2	86.5	86.3
VGG 19 NN	90.9	84.4	84.4	84.4	84.4
VGG 19 KNN	90.8	83.1	83.0	83.8	83.1
VGG 19 NB	80.5	80.0	80.0	80.0	80.0
VGG 19 Adaboost	90.8	83.8	83.7	83.9	83.8
VGG 16 LR	88.9	83.1	83.1	83.1	83.1
VGG 16 SVM	90.2	84.4	84.3	85.0	84.4
VGG 16 SGD	80.6	80.6	80.6	80.7	80.6
VGG 16 NN	90.9	83.8	83.7	83.9	83.8
VGG 16 KNN	90.5	83.8	83.7	83.8	83.8
VGG 16 NB	81.6	80.6	80.6	80.7	80.6
VGG 16 Adaboost	89.8	82.5	82.5	82.7	82.5
MFO-CNN	**95.31**	**95.3**	**91.39**	**94.32**	**92.19**

The Accuracy of proposed MFO-CNN classifier is 12%, 12% and 16% higher than the VCG16 KNN, VCG19 KNN and inception V3 KNN classifier respectively. The Accuracy of proposed MFO-CNN classifier is 15%, 16% and 20% higher than the VCG16 NB, VCG19 NB and inception V3 NB classifier respectively. The Accuracy of proposed MFO-CNN classifier is 13%, 12% and 23% higher than the VCG16 Adaboost, VCG19 Adaboost and inception V3 Adaboost classifier respectively.

F measure of MFO-CNN classifier is 9%, 6% and 8% higher than the VCG16 LR, VCG19 LR

and inception V3 LR classifier respectively. F measure of proposed MFO-CNN classifier is 7%, 8% and 10% higher than the VCG16 SVM, VCG19 SVM and inception V3 SVM classifier respectively. F measure of proposed MFO-CNN classifier is 11%, 5% and 10% higher than the VCG16 SGD, VCG19 SGD and inception V3 SGD classifier respectively. F measure of proposed MFO-CNN classifier is 8%, 7% and 12% higher than the VCG16 NN, VCG19 NN and inception V3 NN classifier respectively. The F measure of proposed MFO-CNN classifier is 8%, 9% and 13% higher than the VCG16 KNN, VCG19 KNN and inception V3 KNN classifier respectively. The F measure of proposed MFO-CNN classifier is 11%, 12% and 17% higher than the VCG16 NB, VCG19 NB and inception V3 NB classifier respectively. The F measure of proposed MFO-CNN classifier is 9%, 8% and 20% higher than the VCG16 Adaboost, VCG19 Adaboost and inception V3 Adaboost classifier respectively.

The Precession MFO-CNN classifier is 11%, 9% and 11% higher than the VCG16 LR, VCG19 LR and inception V3 LR classifier respectively. The Precession of proposed MFO-CNN classifier is 9%, 10% and 12% higher than the VCG16 SVM, VCG19 SVM and inception V3 SVM classifier respectively. The Precession of proposed MFO-CNN classifier is 14%, 8% and 13% higher than the VCG16 SGD, VCG19 SGD and inception V3 SGD classifier respectively. The Precession of proposed MFO-CNN classifier is 11%, 10% and 15% higher than the VCG16 NN, VCG19 NN and inception V3 NN classifier respectively. The Precession of proposed MFO-CNN classifier is 11%, 11% and 15% higher than the VCG16 KNN, VCG19 KNN and inception V3 KNN classifier respectively. The Precession of proposed MFO-CNN classifier is 14%, 15% and 19% higher than the VCG16 NB, VCG19 NB and inception V3 NB classifier respectively. The Precession of proposed MFO-CNN classifier is 12%, 11% and 23% higher than the VCG16 Adaboost, VCG19 Adaboost and inception V3 Adaboost classifier respectively. Recall of MFO-CNN classifier is 9.8 %, 8% and 9% higher than the VCG16 LR, VCG19 LR and inception V3 LR classifier respectively. The Recall of proposed MFO-CNN classifier is 8%, 9% and 11% higher than the VCG16 SVM, VCG19 SVM and inception V3 SVM classifier respectively. The Recall of proposed MFO-CNN classifier is 12%, 6% and 11% higher than the VCG16 SGD, VCG19 SGD and inception V3 SGD classifier respectively. The Recall of proposed MFO-CNN classifier is 9%, 8% and 13% higher than the VCG16 NN, VCG19 NN and inception V3 NN classifier respectively. The Recall of proposed MFO-CNN classifier is 9%, 9% and 13% higher than the VCG16 KNN, VCG19 KNN and inception V3 KNN classifier respectively. The Recall of proposed MFO-CNN classifier is 12%, 13% and 18% higher than the VCG16 NB, VCG19 NB and inception V3 NB classifier respectively. The Recall of proposed MFO-CNN classifier is 10%, 9% and 21% higher than the VCG16 Adaboost, VCG19 Adaboost and inception V3 Adaboost classifier respectively. Fig. 10a-g shows the comparative analysis of proposed MFO-CNN classifier with existing LR, SVM, SGD, NN, KNN, NB and Adaboost classifiers respectively.

Fig. 10. Performance comparison of proposed MFO-CNN classifier over (a) LR (b) SVM (c) SGD (d) NN (e) KNN (f) NB (g) Adaboost classifiers

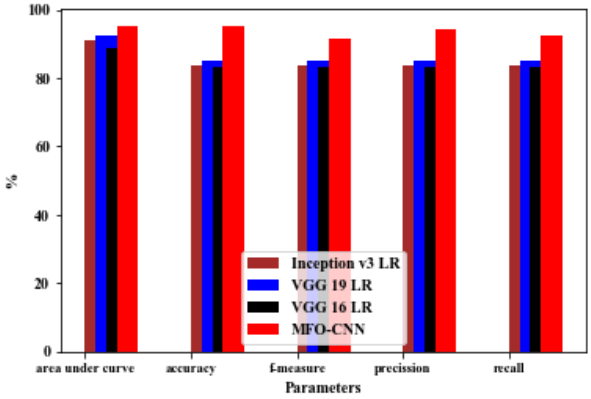

a

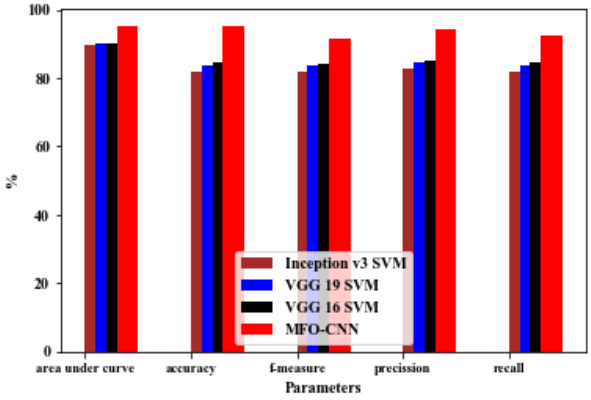

b

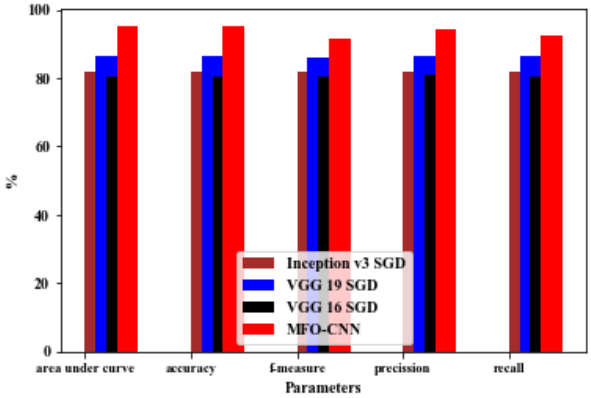

c

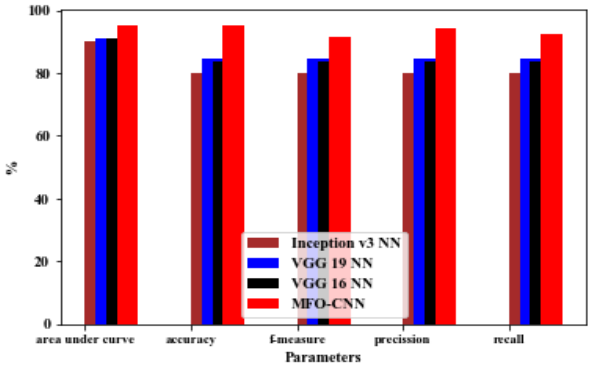

d

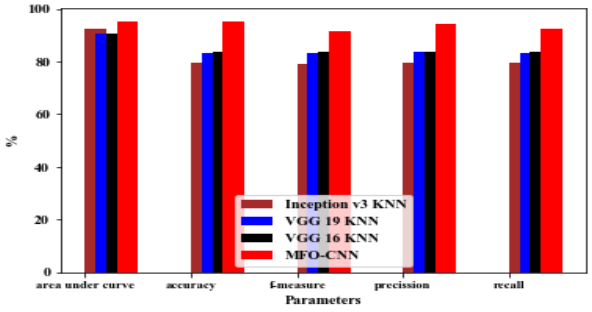

e

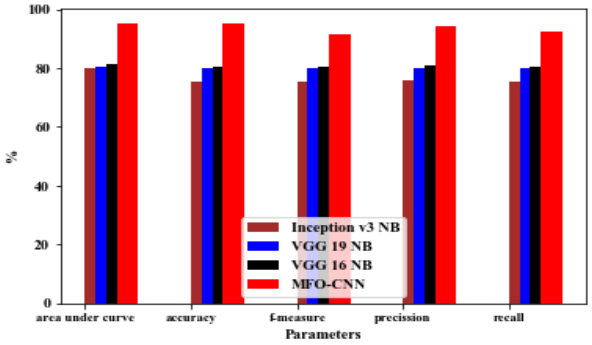

f

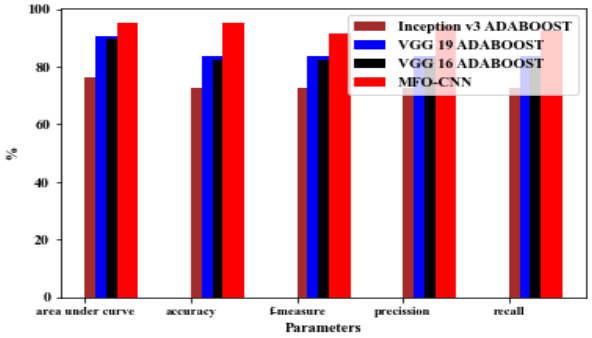

g

6. CONCLUSION

A hybrid optimal machine learning technique (HOML-SL) is proposed for detecting the disease in sugarcane. A nonlinear cluster based optimization algorithm is used for segmenting the disease from the leaves. Then, a cross layer optimization based optimal feature selection technique used to select optimal and best feature among multiple features. Finally, we used MFO-CNN classifier for disease prediction and classification into multi-levels such mosaic, red rot, rings spot, grassy shoot and health types. The average accuracy of proposed MFO-CNN classifier is 12.8%, 11.7%, 16.4% higher than the existing method such as VGG 16, VGG 19 and Inception IV3 with state-of-art classifiers respectively. The average area under curve of proposed MFO-CNN classifier is 7.8%, 6.2%, 9.4% higher than the existing method such as VGG 16, VGG 19 and Inception IV3. The average precision of proposed MFO-CNN classifier is 11.4%, 10.5%, 15.4% higher than the existing method such as VGG 16, VGG 19 and Inception IV3. The average F-measure of proposed MFO-CNN classifier is 9%, 7.8%, 12.8% higher than the existing method such as VGG 16, VGG 19 and Inception IV3. The average recall of proposed MFO-CNN classifier is 8.7%, 9%, 13.7% higher than the existing method such as VGG 16, VGG 19 and Inception IV3.

REFERENCES

Fontaniella, B., Vicente, C., Legaz, M.E., de Armas, R., Rodríguez, C.W., Martínez, M., Piñón, D., Acevedo, R. and Solas, M.T., 2003. Yellow leaf syndrome modifies the composition of sugarcane juices in polysaccharides, phenols and polyamines. Plant Physiology and Biochemistry, 41(11-12), pp.1027-1036.

Miura, T., Niswati, A., Swibawa, I.G., Haryani, S., Gunito, H. and Kaneko, N., 2013. No tillage and bagasse mulching alter fungal biomass and community structure during decomposition of sugarcane leaf litter in Lampung Province, Sumatra, Indonesia. Soil Biology and Biochemistry, 58, pp.27-35.

Singh, N., Somai, B.M. and Pillay, D., 2004. Smut disease assessment by PCR and microscopy in inoculated tissue cultured sugarcane cultivars. Plant Science, 167(5), pp.987-994.

Caballero, B., Trugo, L.C. and Finglas, P.M., 2003. Encyclopedia of food sciences and nutrition. Academic.

Ratnasari, E.K., Mentari, M., Dewi, R.K. and Ginardi, R.H., 2014, September. Sugarcane leaf disease detection and severity estimation based on segmented spots image. In Proceedings of International Conference on Information, Communication Technology and System (ICTS) 2014 (pp. 93-98). IEEE.

Xie, Y., Wang, M., Xu, D., Li, R. and Zhou, G., 2009. Simultaneous detection and identification of four sugarcane viruses by one-step RT-PCR. Journal of virological methods, 162(1-2), pp.64-68.

Glynn, N.C., Gilbert, R.A., Comstock, J.C. and Davis, M.J., 2010. Transmission of a Sugarcane yellow leaf virus resistance transgene to sexual progeny and screening by kanamycin inoculation. Field crops research, 119(2-3), pp.308-313.

Chandra, A., Keizerweerd, A.T., Que, Y. and Grisham, M.P., 2015. Loop-mediated isothermal amplification (LAMP) based detection of Colletotrichum falcatum causing red rot in sugarcane. Molecular biology reports, 42(8), pp.1309-1316.

Madugula, S. and Gali, U.D., 2017. Virus indexing for Sugarcane Yellow Leaf Virus (SCYLV) in field varieties and in vitro regenerated plantlets of sugarcane. Australasian Plant Pathology, 46(5), pp.433-439.

Roddee, J., Kobori, Y. and Hanboonsong, Y., 2018. Multiplication and distribution of sugarcane white leaf phytoplasma transmitted by the leafhopper, Matsumuratettix hiroglyphicus (Matsumura) (Hemiptera: Cicadellidae), in infected sugarcane. Sugar Tech, 20(4), pp.445-453

Yano, I.H., Alves, J.R., Santiago, W.E. and Mederos, B.J., 2016. Identification of weeds in sugarcane fields through images taken by UAV and random forest classifier. IFAC-PapersOnLine, 49(16), pp.415-420.

Kumar, S., Mishra, S. and Khanna, P., 2017. Precision sugarcane monitoring using SVM classifier. Procedia Computer Science, 122, pp.881-887.

Dewanti, P., Widuri, L.I., Ainiyati, C., Okviandari, P. and Sugiharto, B., 2016. Elimination of SCMV (sugarcane Mozaik virus) and rapid propagation of virus-free sugarcane (Saccharum officinarum L.) using somatic embryogenesis. Procedia Chemistry, 18, pp.96-102.

Militante, S.V. and Gerardo, B.D., 2019, December. Detecting Sugarcane Diseases through Adaptive Deep Learning Models of Convolutional Neural Network. In 2019 IEEE 6th International Conference on Engineering Technologies and Applied Sciences (ICETAS) (pp. 1-5). IEEE.

Zhou, D., Guo, J., Xu, L., Gao, S., Lin, Q., Wu, Q., Wu, L. and Que, Y., 2014. Establishment and application of a loop-mediated isothermal amplification (LAMP) system for detection of cry1Ac transgenic sugarcane. Scientific reports, 4(1), pp.1-8.

Shen, W., Xu, G., Sun, L., Zhang, L. and Jiang, Z., 2016. Development of a loop‐mediated isothermal amplification assay for rapid and sensitive detection of Sporisorium scitamineum in sugarcane. Annals of Applied Biology, 168(3), pp.321-327.

Quoc, N.B., Xuan, N.T.T., Phuong, N.D.N., Trang, H.T.T., Chau, N.N.B., Duong, C.A. and Dickinson, M., 2021. Development of loop mediated isothermal amplification assays for the detection of sugarcane white leaf disease. Physiological and Molecular Plant Pathology, p.101595.

Yan, S.L., Lehrer, A.T., Hajirezaei, M.R., Springer, A. and Komor, E., 2008. Modulation of carbohydrate metabolism and chloroplast structure in sugarcane leaves which were infected by Sugarcane Yellow Leaf Virus (SCYLV). Physiological and Molecular Plant Pathology, 73(4-5), pp.78-87.

Nasanit, R., Tantirungkij, M. and Limtong, S., 2015. The assessment of epiphytic yeast diversity in sugarcane phyllosphere in Thailand by culture-independent method. Fungal biology, 119(12), pp.1145-1157.

Lin, L.H., Ntambo, M.S., Rott, P.C., Wang, Q.N., Lin, Y.H., Fu, H.Y. and Gao, S.J., 2018. Molecular detection and prevalence of Xanthomonas albilineans, the causal agent of sugarcane leaf scald, in China. Crop Protection, 109, pp.17-23.

Zhang, Y., Huang, Q., Yin, G., Jia, R., Lee, S., Xiong, G., Yu, N., Pennerman, K.K., Liu, Z. and Zhang, S., 2015. Genetic diversity of viruses associated with sugarcane

mosaic disease of sugarcane inter-specific hybrids in China. European journal of plant pathology, 143(2), pp.351-361.

Mollov, D., Maroon-Lango, C. and Kuniata, L., 2016. Detection by next generation sequencing of a multi-segmented viral genome from sugarcane associated with Ramu stunt disease. Virus genes, 52(1), pp.152-155.

Avellaneda, M.C., Parco, A.P., Hoy, J.W. and Baisakh, N., 2018. Putative resistance-associated genes induced in sugarcane in response to the brown rust fungus, Puccinia melanocephala and their use in genetic diversity analysis of Louisiana sugarcane clones. Plant Gene, 14, pp.20-28.

Hamonts, K., Trivedi, P., Grinyer, J., Holford, P., Drigo, B., Anderson, I.A. and Singh, B.K., 2018. Yellow Canopy Syndrome in sugarcane is associated with shifts in the rhizosphere soil metagenome but not with overall soil microbial function. Soil Biology and Biochemistry, 125, pp.275-285.

Li, W.F., Shan, H.L., Zhang, R.Y., Wang, X.Y., Yang, K., Luo, Z.M., Yin, J., Cang, X.Y., Li, J. and Huang, Y.K., 2018. Identification of resistance to Sugarcane streak mosaic virus (SCSMV) and Sorghum mosaic virus (SrMV) in new elite sugarcane varieties/clones in China. Crop Protection, 110, pp.77-82.

Ukoskit, K., Posudsavang, G., Pongsiripat, N., Chatwachirawong, P., Klomsa-Ard, P., Poomipant, P. and Tragoonrung, S., 2019. Detection and validation of EST-SSR markers associated with sugar-related traits in sugarcane using linkage and association mapping. Genomics, 111(1), pp.1-9.

XU, J.S., DENG, Y.Q., CHENG, G.Y., ZHAI, Y.S., Lei, P.E.N.G., Meng, D.O.N.G., Qian, X.U. and YANG, Y.Q., 2019. Sugarcane mosaic virus infection of model plants Brachypodium distachyon and Nicotiana benthamiana. Journal of Integrative Agriculture, 18(10), pp.2294-2301.

Srivastava, S., Kumar, P., Mohd, N., Singh, A. and Gill, F.S., 2020. A Novel Deep Learning Framework Approach for Sugarcane Disease Detection. SN Computer Science, 1(2), pp.1-7.

Oliveira, I.A., Layla de Sá, A.M., Gonçalves, M.C., de Jesus Pereira, H., de Alcântara Neto, F., da Silva Matos, K. and Beserra Jr, J.E.A., 2020. A survey of causal agents associated with sugarcane yellowing in Northeast Brazil. Crop Protection, 138, p.105326.

De Torres, R., Cueva, F.D. and Balendres, M.A., 2020. First report on the detection of fumonisin biosynthetic (FUM1) gene in Fusarium verticillioides and F. proliferatum associated with sugarcane diseases. Indian Phytopathology, pp.1-5.

Srivastava, S., Kumar, P., Mohd, N., Singh, A. and Gill, F.S., 2020. A Novel Deep Learning Framework Approach for Sugarcane Disease Detection. SN Computer Science, 1(2), pp.1-7.